ELSEVIER

Development and characterization of a TES optical imaging array for astrophysics applications

J. Burney[a,*], T.J. Bay[a], P.L. Brink[a], B. Cabrera[a], J.P. Castle[a], R.W. Romani[a], A. Tomada[a], S.W. Nam[b], A.J. Miller[b], J. Martinis[b], E. Wang[c], T. Kenny[c], B.A. Young[d]

[a] Department of Physics, Stanford University, Stanford, CA 94306, USA
[b] National Institute of Standards and Technology (NIST), Boulder, CO 80303, USA
[c] Department of Mechanical Engineering, Stanford University, Stanford, CA 94306, USA
[d] Department of Physics, Santa Clara University, Santa Clara, CA 95053, USA

Abstract

Our research group has successfully developed photon detectors capable of both time-stamping and energy-resolving individual photons at very high rates in a wide band from the near-IR through optical and into the near-UV. We have fabricated 32-pixel arrays of these Transition-Edge Sensor (TES) devices and have mounted them in an adiabatic demagnetization refrigerator equipped with windows for direct imaging. We have characterized single pixel behavior; we have also begun operating multiple pixels simultaneously, starting the scaling process towards use of the full array. We emphasize the development of a metalized mask for our array that blocks photons from hitting the inter-pixel areas and reflects them onto the TESs. We also present calibration data on detector resolution, electronics noise, and optical alignment.
© 2003 Published by Elsevier B.V.

1. Introduction

Superconducting detector arrays have recently made it possible to both time-stamp and energy-resolve arriving photons, opening a new realm of observational capability. Both superconducting tunnel junctions (STJs) and Transition Edge Sensors (TESs) have been used in preliminary astrophysics observations (for example, see Refs. [1,2]). These have provided a glimpse into the potential impact of an imaging system made of TESs. To that end, we have taken the first steps towards packaging TESs into imaging arrays in a compact and convenient observing unit.

Our array is housed in a Janis adiabatic demagnetization refrigerator (ADR). The cryostat has a base temperature under 50 mK and a nominal heat load of 300 nW on the base stage with all pixels wired. This corresponds to a

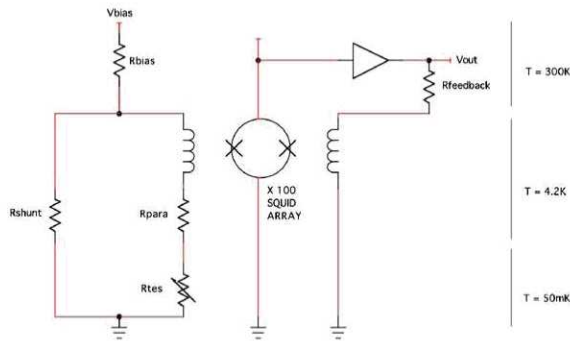*Corresponding author.
E-mail address: burney@stanford.edu (J. Burney).

Fig. 1. Schematic of TES and SQUID amplifier circuit, showing the temperature of each element (for noise calculations). Typical values: $R_{shunt} = 3$ mΩ, $R_{para} = 4.6$ mΩ, $R_{bias} = R_{feedback} = 3.6$ kΩ.
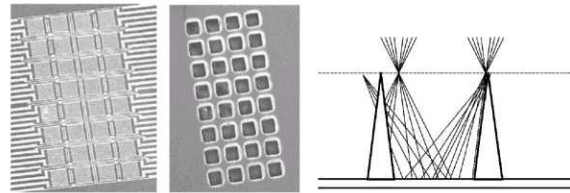

Fig. 2. Left, 32-pixel W TES array; center, top view of metalized reflection mask; right, schematic elevation of reflection mask function.

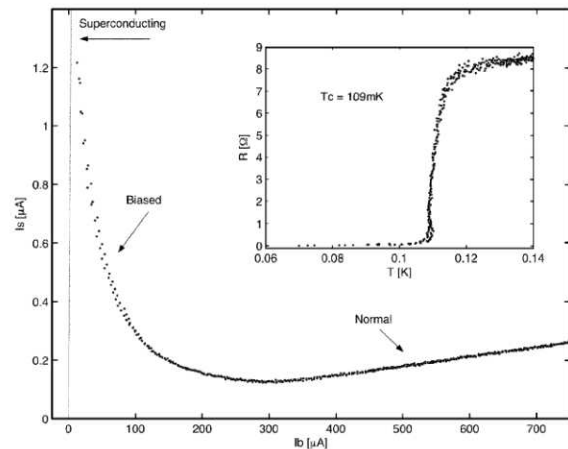Fig. 3. I_{bias} vs. I_{sensor} for a W TES, showing superconducting, biased (at 68 μA), and normal regions. The inset plot of R vs. T for the same sensor shows the sharp superconducting-normal transition at $T_c = 109$ mK.

run-time of 10 h for devices with a critical temperature of 100 mK, allowing for a night of observing well below T_c without having to regenerate the magnet. Each TES is inductively coupled to a SQUID amplifier circuit (see Fig. 1). We read out signals via a PCI-based digital feedback system and stream data directly to disk. The SQUID arrays and companion electronics mentioned are fabricated by NIST. Light enters the dewar via filter-glass windows (sapphire at room temperature, KG3 at 77 K and 4.2 K), and is focused onto the array with a microscope objective (f/15) attached to the 4.2 K window.

2. Device characterization

Our arrays are photolithographically patterned 40 nm thin W films. They consist of 4×8 individual TESs, each 20 μm $\times$ 20 μm, with 1.5 μm-wide aluminum voltage bias rails. We have placed a first-generation reflection mask over our array (see Fig. 2). The mask both blocks incoming photons from hitting the device rails and reflects them onto the sensor. This effectively increases our fill-factor, ultimately making the array a much more useful imaging tool.

Each TES has a T_c of ~ 109 mK. Fig. 3 shows some of the critical parameters for our devices. With these sensors, we have achieved energy resolution across the optical band of ~ 0.5 eV.

Fig. 4 shows both averaged traces of individual red (1.91 eV) and green (2.33 eV) laser photons, as well as an energy spectrum for one pixel illuminated by the green photons. The ratios of the collected pulse energies work out as expected (0.83 experiment vs. 0.82 theory), indicating a linear detector response over the energy range measured. At both wavelengths, the integrated pulse energy indicates an overall energy collection efficiency of 43%. This agrees with previous results on similar devices [3].

Our resolution, however, is far worse than in previous work with TESs. Single pixels have been shown to have 0.15 eV resolution [4], and individual pixels as part of an array have been shown to have 0.23 eV [5]. To understand this discrepancy, we must examine intrinsic, electronic, and optical
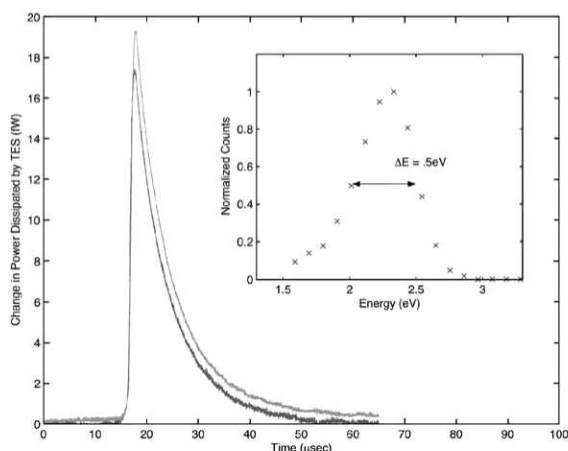
Fig. 4. Averaged traces of red (smaller pulse) and green (larger pulse) photons directly absorbed by W TES via cryostat windows. The inset figure shows a spectrum of green photons taken with NIST digital acquisition system.

(position-dependence, photon and RF background at the sensor stage, etc.) noise sources.

3. Noise analysis

In the simplest model, the intrinsic resolution of a TES is limited by phonon noise according to Ref. [6], and is given by $\Delta E_{\text{fwhm}} = (\frac{2.355}{\varepsilon})\sqrt{4k_{\text{b}}T_{\text{c}}P_0\tau_{\text{etf}}\sqrt{n/2}}$ where ε is the collection efficiency of the detector, P_0 is the quiescent operating (bias) power, τ_{etf} is the pulse fall-time, and n is the thermal coupling power-law exponent (in this case, $n = 5$) [3]. For our current devices ($\varepsilon = 0.43$, $P_0 = 100$ fW, $\tau_{\text{etf}} = 8$ μs), this gives $\Delta E_{\text{fwhm}} = 0.1$ eV. A few changes to our experimental setup should improve this intrinsic resolution by a factor of 2: (a) we plan to tune the T_{c} of our devices down using ion implantation [7], (b) we will begin fabricating devices on SiN membranes, minimizing losses to the substrate. A collection efficiency of 0.8 and an adjusted T_{c} of 95 mK would result in $\Delta E_{\text{fwhm}} = 0.04$ eV.

This intrinsic resolution, however, does not take into account noise from the accompanying circuitry. The model put forth by Figueroa [8] attempts to do this: with our resistor values and device parameters, it predicts $\Delta E_{\text{fwhm}} = 0.14$ eV. As above, however, assuming a tuned T_{c} and doubled efficiency in this model results in $\Delta E_{\text{fwhm}} = 0.05$ eV.

The Figueroa scheme, however, assumes optimal filtering of the pulses, which we have not performed. As a test of our readout chain (including electronics noise and non-optimal filtering), we closed the cryostat window and summed the output of the static TES-SQUID circuit with a known pulse signal of similar parameters to optical photons. A calculation of the Johnson noise from the bias, parasitic, shunt, and biased sensor resistances, as well as the SQUID noise (measured independently) gives an estimate spread on these non-optimally filtered mock pulses of ~ 0.35 eV. We measured ΔE_{fwhm} to be 0.37 eV.

Thus, we believe that we understand the electronic and readout components of our noise. A plausible source of the remaining degraded energy resolution is the presence of cryodeposits on the cold stage. Such deposits, generated during repeated cycles to room temperature while debugging, create position sensitivity in the detector response. The position-dependence produces low-energy "smearing" in the energy PSF (see Fig. 4 inset).

4. Multi-pixel operation

We have operated two side-by-side pixels in unison and have seen that cross-talk is small, if not negligible. We are currently working to probe the behavior of our array more directly with a carefully aligned fiber. Using the focusing optic in our dewar, light from a 50 μm-core fiber will produce a 3 μm spot, which easily fits within one pixel, especially with the confining aid of the reflection mask. We therefore expect to measure cross-talk, collection efficiency, and position dependence much more precisely in the near future.

5. Conclusion

We have completed the first stages of characterization of an imaging array of TESs in an ADR

equipped with windows for direct imaging with high-detector quantum efficiency. In its initial operation, the system is behaving as expected, and we believe that we will have greatly improved energy resolution in the immediate future. Furthermore, we have begun the scaling process to multiple pixels, with success.

Acknowledgements

References

[1] D. Steeghs, et al., Mon. Not. R. Astron. Soc. 323 (2002) 484.
[2] R.W. Romani, et al., Astrophys. J. 563 (2001) 221.
[3] A.J. Miller, Stanford University Disseration, 2001.
[4] B. Cabrera, et al., App. Phys. Lett. 73 (1998) 735.
[5] R.W. Romani, et al., Astrophys. J. 521 (1999) 153.
[6] K. Irwin, App. Phys. Lett. 66 (1995) 1998.
[7] B.A. Young, et al., J. App. Phys. 86 (2002) 6975.
[8] E. Figueroa-Feliciano, Stanford University Dissertation, 2001.